Environmental Science & Technology

pubs.acs.org/est

Article

Atmospheric Mercury Concentrations and Isotopic Compositions Impacted by Typical Anthropogenic Mercury Emissions Sources

Chuan Wang, Shaochen Yang, Ruolan Li, Junyao Yan, Yanxin Hu, Chuyan Lai, Zhonggen Li, Ping Li,* Leiming Zhang, and Xinbin Feng

Cite This: *Environ. Sci. Technol.* 2024, 58, 16855−16866

Read Online

ACCESS | Metrics & More | Article Recommendations | Supporting Information

ABSTRACT: Coal-fired power plants (CFPPs) and cement plants (CPs) are important anthropogenic mercury (Hg) emission sources. Mercury speciation profiles in flue gas are different among these sources, leading to significant variations in local atmospheric Hg deposition. To quantify the impacts of Hg emissions from CFPPs and CPs on local-scale atmospheric Hg deposition, this study determined concentrations and isotopes of ambient gaseous elemental mercury (GEM), particulate-bound mercury (PBM), and precipitation total Hg (THg) at multiple locations with different distances away from a CFPP and a CP. Higher concentrations of GEM and precipitation THg in the CFPP area in summer were caused by higher Hg emission from the CFPP, resulting from higher electricity demand. Higher concentrations of GEM, PBM, and precipitation THg in the CP area in winter compared to those in summer were related to the higher output of cement. Atmospheric Hg concentration peaked near the CFPP and CP and decreased with distance from the plants. Elevated GEM concentration in the CFPP area was due to flue gas Hg^0 emissions, and high PBM and precipitation Hg concentrations in the CP area were attributed to divalent Hg emissions. It was estimated that Hg emissions from the CFPP contributed 58.3 ± 20.9 and 52.3 ± 25.9% to local GEM and PBM, respectively, and those from the CP contributed 47.0 ± 16.7 and 60.0 ± 25.9% to local GEM and PBM, respectively. This study demonstrates that speciated Hg from anthropogenic emissions posed distinct impacts on the local atmospheric Hg cycle, indicating that Hg speciation profiles from these sources should be considered for evaluating the effectiveness of emission reduction policies. This study also highlights the Hg isotope as a useful tool for monitoring environmental Hg emissions.

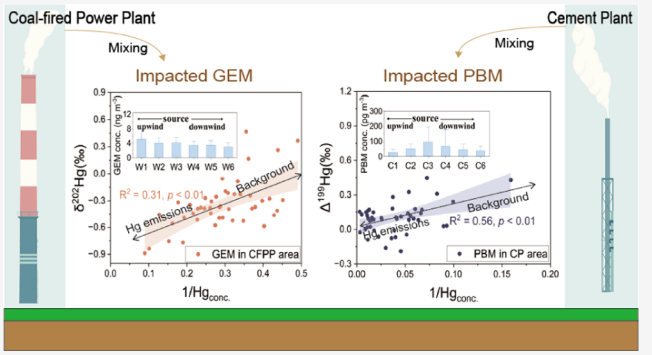

KEYWORDS: *atmospheric mercury, anthropogenic emissions, seasonal-spatial variation, mercury isotope, source apportionment*

1. INTRODUCTION

Atmospheric mercury (Hg) is a globally pervasive and toxic pollutant. Atmospheric Hg is operationally defined in three different forms: gaseous elemental mercury (GEM or Hg^0), gaseous oxidized mercury (GOM), and particulate-bound mercury (PBM).[1] Mercury directly emitted into the atmosphere, whether from anthropogenic or natural sources, is predominantly in the form of Hg^0.[2] However, the proportion of divalent Hg (Hg^{II}) emitted from anthropogenic sources has gradually increased in recent decades.[3,4] Although the total Hg emissions from anthropogenic sources were gradually decreasing due to the implementation of a number of pollution control measures,[5] the increase in the proportion of Hg^{II} in flue gas may partly offset the impact of reduced Hg emissions in a local-scale environment because of the faster deposition rate of GOM and PBM than GEM.[6] The deposited Hg in terrestrial and aquatic ecosystems has the potential to undergo methylation by microorganisms to form methylmercury (MeHg), a species that can be bioaccumulated in the food chain and poses a health threat to ecosystems and human health.[7,8] Hence, a comprehensive understanding of the sources, transport processes, and fates of speciated atmospheric Hg is crucial for assessing Hg impacts on ecosystem and human health.

Coal-fired power plants (CFPPs) and cement plants (CPs) are the predominant sectors of anthropogenic Hg emissions in China.[3,9,10] In 2015, cement production emerged as the largest source of Hg emission in China, emitting 144 Mg Hg,[11] while CFPPs constituted the second largest source, emitting 73 Mg Hg.[12] Up to 84.5% and approximately 25% of the total Hg emission amounts mentioned above are in the form of Hg^{II} from cement production and CFPPs, respectively.[11] This implies that

Received: July 25, 2024
Revised: August 30, 2024
Accepted: August 30, 2024
Published: September 10, 2024

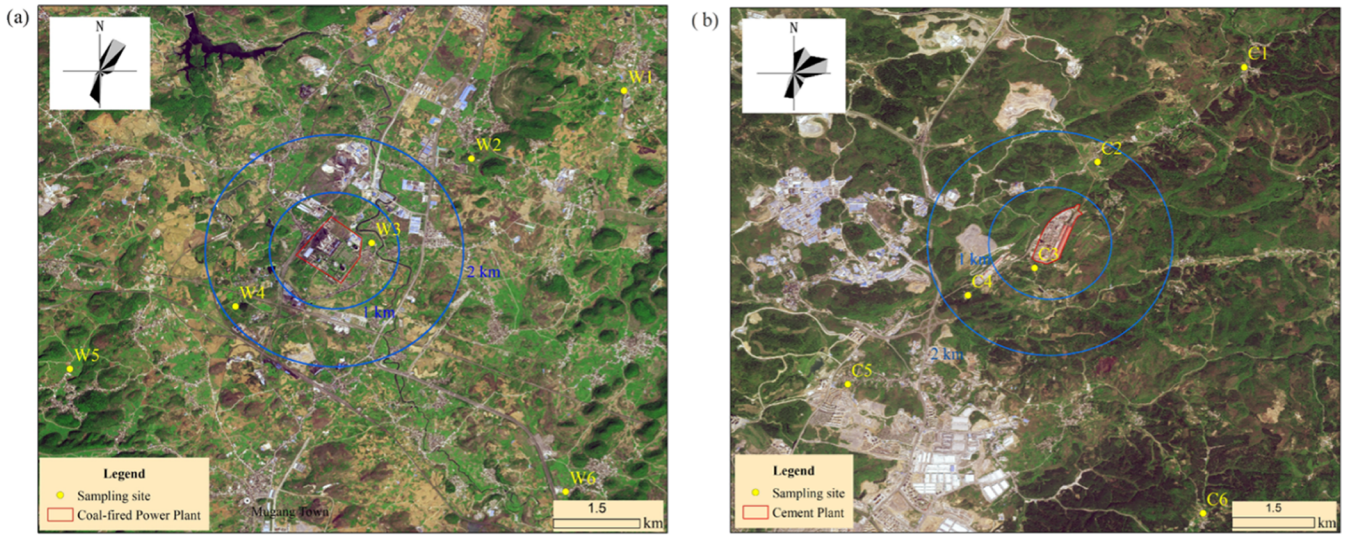

Figure 1. Spatial distribution of sampling sites in the coal-fired power plant area (a) and cement plant area (b). Point W1 (or C1) to W5 (or C5) were within 5 km of the coal-fired power plant (or cement plant) in the prevailing wind direction and point W6 (or C6) (~5 km away from point source) was set as the control site.

Hg deposition from CPs is much higher than that from CFPPs in China due to higher cement-related Hg^{II} emissions. Considering that the sum of atmospheric Hg emissions from CFPPs and CPs accounted for approximately 42% of the national total emissions,[3,10] it is essential to gain a complete understating of the speciated Hg emissions from these two source sectors to comprehensively assess the subsequent environmental impacts.

Mercury stable isotopes have been used to trace the sources and biogeochemical processes of different forms of atmospheric Hg.[13−16] Mercury can undergo mass-dependent fractionation (MDF, reported as δ^{202}Hg) and mass-independent fractionation (MIF) in the natural environment. MIF includes odd-MIF (reported as Δ^{199}Hg and Δ^{201}Hg) and even-MIF (reported as Δ^{200}Hg and Δ^{204}Hg).[17] Both biotic and abiotic reactions, including reduction, methylation/demethylation, sorption, and evaporation, can induce MDF, while odd-MIF is mainly triggered by photochemical reactions.[18] In addition, even-MIF is mainly observed in atmospheric samples and is caused by upper stratospheric redox reactions.[19] Mercury isotope compositions of anthropogenic sources, such as coal combustion (residential and power plants),[20,21] cement production,[22] nonferrous metals[23] and biomass burning,[13,24] and background atmospheric Hg speciation[15,16,19,25] were distinguished in previous studies. Therefore, atmospheric Hg speciation from emission sources can be quantified through the Hg isotopes. However, only a few studies reported ambient atmospheric Hg concentrations and isotopic compositions surrounding CFPPs and associated source apportionment analysis,[26−28] and no study focused on areas surrounding CPs. To date, the extent of impacts of Hg emission sources with distinct Hg speciation profiles on atmospheric Hg isotopic compositions at local scales is still unclear.

To fill the knowledge gaps mentioned above, in this study, we collected GEM, PBM, and precipitation samples at multiple sites in the vicinity of a CFPP and a CP in southwest China. Ambient concentrations and isotopic compositions of speciated atmospheric Hg were then determined to assess the impacts of emission sources on atmospheric Hg at the local scale. Knowledge gained from this study would improve the cognition of geochemical processes involving atmospheric Hg and elucidate impacts of changing anthropogenic Hg emissions on the natural environment.

2. MATERIALS AND METHODS

2.1. Study Area and Sample Collection. A CFPP and a CP in Guizhou province of southwest China were selected for investigation. The CFPP (26°12′53.01″ N, 105°41′31.65″ E), located in the southwest of Guizhou province, China, is equipped with selective catalytic reduction (SCR), electrostatic precipitator (ESP) and wet flue gas desulphurization systems (WFGD). The CP (26°32′22.57″ N, 106°53′32.73″ E), located in the central part of Guizhou province, China, is operated by preheater/precalciner kilns with two production capacity lines of 5000 tons of clinker per day. Considering prevailing wind directions and potentially impacted zones by flue gas stacks, six sites within 5 km radius of each plant were selected for field sampling, as shown in Figure 1. Note that there were no other significant Hg sources in these areas.

A total of 333 samples were collected from summer 2021 to spring 2022 in the CFPP area and from autumn 2021 to summer 2022 in the CP area, which included 189 GEM samples, 96 PBM samples, and 48 precipitation samples. GEM samples were collected using chlorine-impregnated activated carbon (CLC) and pumped with the gas flow at about 2.5 L/min.[29] PBM samples were collected on precombusted (500 °C for 3 h) quartz fiber filters (203 mm × 254 mm, Whatman QM-A) using high-volume total suspended particles (TSP) samplers at a flow of 1000 L/min.[30] The precipitation samples were collected with Teflon films and stored in purified, Hg-free brown glass bottles. The collected precipitation samples were acidified using 0.5% (v:v) ultrapure hydrochloric acid in the field and transported back to the laboratory for cold storage before subsequent analysis.[31]

2.2. Sample Processing and Quality Assurance/Quality Control. To fulfill the criteria for Hg isotope analysis, Hg in precipitation needs to be enriched based on the method established by Li et al.[32] Mercury in CLC and quartz fiber filters was preconcentrated through combustion in a quartz tube, which was subsequently concentrated into 5 mL of 40% HNO_3/HCl mixed trapping solution (v/v, 2:1).[33] For acid-trapping

https://doi.org/10.1021/acs.est.4c07649
Environ. Sci. Technol. 2024, 58, 16855−16866

Table 1. Statistics of Hg Concentrations and Isotope Compositions of GEM, PBM, and Precipitation Samples

area	sample type	parameter	Hg conc.[a]	δ^{202}Hg (‰)	Δ^{199}Hg (‰)	Δ^{200}Hg (‰)	Δ^{201}Hg (‰)
CFPP	GEM	*n*	94	48			
		mean ± 1 SD	3.91 ± 1.80	0.35 ± 0.28	−0.08 ± 0.07	−0.03 ± 0.06	−0.11 ± 0.09
		range	2.04−11.2	−0.89 to 0.47	−0.28 to 0.01	−0.25 to 0.06	−0.40 to 0.06
	PBM	*n*	48	48			
		mean ± 1 SD	44.9 ± 32.3	−1.07 ± 0.85	0.37 ± 0.34	0.09 ± 0.05	0.21 ± 0.22
		range	8.90−140	−0.89 to 0.32	−0.45 to 0.03	−0.12 to 0.06	−0.45 to 0.02
	precipitation	*n*	24	24			
		mean ± 1 SD	14.9 ± 6.97	−0.64 ± 0.34	0.54 ± 0.38	0.14 ± 0.06	0.46 ± 0.31
		range	6.80−31.2	−1.26 to 0.06	0.13−1.62	0.05−0.31	0.06−1.26
CP	GEM	*n*	95	48			
		mean ± 1 SD	4.28 ± 2.26	−0.28 ± 0.28	−0.10 ± 0.12	−0.01 ± 0.03	−0.12 ± 0.11
		range	1.10−15.7	−0.89 to 0.32	−0.45 to 0.03	−0.12 to 0.06	−0.45 to 0.02
	PBM	*n*	48	48			
		mean ± 1 SD	55.0 ± 65.6	−0.71 ± 0.77	0.11 ± 0.14	0.05 ± 0.06	0.06 ± 0.13
		range	6.30−338	−2.25 to 0.74	−0.19 to 0.49	−0.06 to 0.17	−0.21 to 0.42
	precipitation	*n*	24	24			
		mean ± 1 SD	51.1 ± 128	−0.92 ± 0.61	0.24 ± 0.22	0.13 ± 0.06	0.17 ± 0.23
		range	3.64−616	−2.20 to 0.04	−0.13 to 0.65	0.02−0.22	−0.15 to 0.65

[a]Unit: GEM: ng m^{-3}; PBM: pg m^{-3}; precipitation: ng L^{-1}.

solution samples, Hg concentrations were determined by cold vapor atomic fluorescence spectrometry (CVAFS, Tekran 2500). Mercury concentration of each sample was calculated based on the detection of Hg concentration in trapping solution and sampling volume.

Blanks of CLC traps and quartz fiber filters were measured, which showed mean values of 0.23 ± 0.13 ng (1 SD, n = 7) and 0.22 ± 0.17 ng (1 SD, n = 4), accounting for <5% of the total mass of GEM collected by CLC and PBM collected by quartz fiber filters, respectively. Recoveries of CLC traps were tested by pumping into Hg^0 vapor, and the mean value was 100 ± 4% (1 SD, n = 2). Recoveries of enrichment of precipitation samples were tested by adding NIST 3133 to Milli-Q water, and the mean recovery was 109 ± 6% (1 SD, n = 3). To evaluate the recoveries of the pretreatment method, certified reference materials (CRM) GBW07405 (GSS-5, yellow-red soil) were used during combustion, which showed mean recoveries of 96 ± 8% (1 SD, n = 7).

Hg isotope ratios were analyzed by a multicollector inductively coupled plasma mass spectrometry (MC-ICP-MS, Nu-Plasma, U.K.), as described in Yin et al.[34] The MDF and MIF of Hg isotope results are reported in delta notation (δ) and capital delta (Δ) per mil (‰), respectively. The MDF and MIF are calculated as follows:

$$\delta^{xxx}\mathrm{Hg}_{sample}(‰) = [(^{xxx/198}Hg_{sample}/^{xxx/198}\mathrm{Hg}_{NIST3133}) - 1] \times 1000 \quad (1)$$

$$\Delta^{xxx}\mathrm{Hg} = \delta^{xxx}\mathrm{Hg} - \beta_{xxx} \times \delta^{xxx}\mathrm{Hg} \quad (2)$$

where xxx is 199, 200, 201, and 202, and β_{xxx} is 0.2520, 0.5024, and 0.7520 for ^{199}Hg, ^{200}Hg, and ^{201}Hg, respectively. The Hg isotopes of UM-Almadén and GBW07405 were repeatedly measured during the isotopic composition analysis to ensure the accuracy and precision, which were consistent with previously reported values (Table S1).[35] Due to the limited Hg mass of available samples, each sample was measured for the Hg isotope only once. The analytical uncertainty of Hg isotopes was determined as the 2SD of all UM-Almadén standard.

2.3. Ancillary Parameters and Statistical Method. TSP mass concentrations were analyzed to elucidate the impact of environmental factors on the variations of PBM concentration and isotopic compositions. The parameters in this study were independent and analyzed by analysis of variance (ANOVA) or nonparametric test through the IBM SPSS Statistics. Pearson's correlation tests were employed for correlation analysis, and ratios of Δ^{199}Hg/Δ^{210}Hg were obtained by William-York bivariate method regression.

3. RESULTS AND DISCUSSION

3.1. Atmospheric and Precipitation Hg Concentration and Isotopic Composition. Statistical values (mean, SD, and range) of concentrations and isotopic compositions of GEM, PBM, and precipitation total Hg (THg) are summarized in Table 1. Average (±1 SD) GEM and PBM concentrations were 3.94 ± 1.83 ng m^{-3} (n = 94) and 44.9 ± 32.3 pg m^{-3} (n = 48), respectively, in the CFPP area and were 4.28 ± 2.26 ng m^{-3} (n = 95) and 55.0 ± 65.6 pg m^{-3} (n = 48), respectively, in the CP area. The GEM concentrations in the study areas were slightly higher than those in Chinese cities (3.08 ± 0.79 ng m^{-3}),[36] but significantly higher than those in remote areas of China (1.43 ± 0.26 ng m^{-3}),[15] and significantly higher than those in North America and Europe (1.94 ± 0.64 ng m^{-3}),[37] indicating elevated GEM levels caused by flue gas Hg emissions from the CFPP and CP. The PBM concentrations in the study areas were actually lower than those in urban areas of China (74.9 ± 82.9 pg m^{-3}),[14,38] but slightly higher than those in remote areas of China (38.4 ± 35.1 pg m^{-3}), and much higher than the global background value (4.6−11.0 pg m^{-3}).[39]

The precipitation concentrations of THg were 14.9 ± 6.97 ng L^{-1} (n = 24) and 51.1 ± 128 ng L^{-1} (n = 24) in the CFPP and CP areas, respectively. The THg concentration in precipitation in the CFPP area was similar to those in Chinese urban areas (e.g., 13.1 ± 6.76 ng L^{-1} in Guiyang City[40] and 10.5 ± 7.24 ng L^{-1} in Xiamen City[26]) and in Great Lakes area in North America (14.3 ± 5.16 ng L^{-1}),[41] while precipitation THg concentrations in the CP area were much higher. These values were also significantly higher than those in Lhasa, Tibetan Plateau (3.1−8.3 ng L^{-1}).[42]

https://doi.org/10.1021/acs.est.4c07649
Environ. Sci. Technol. 2024, 58, 16855−16866

The elevated THg concentration in precipitation in the CP area was due to high Hg^{II} emissions from cement production.[43]

The δ^{202}Hg, Δ^{199}Hg, and Δ^{200}Hg values of GEM averaged at −0.35 ± 0.28, −0.08 ± 0.07, and −0.03 ± 0.06‰ in the CFPP area, respectively, and averaged at −0.28 ± 0.28, −0.10 ± 0.12, and −0.01 ± 0.03‰ in the CP area, respectively (Table S2). No significant difference in Hg isotopes in GEM was found between the CFPP and CP areas ($p > 0.05$). The δ^{202}Hg and Δ^{199}Hg values were comparable to those at urban sites in China[36,38] and industries areas in China[44] and USA.[41] Mean $\Delta^{200}Hg_{GEM}$ values at these two sites were near zero or slightly negative, similar to previous observations in remote and urban areas in China[15,36,45] and North America.[41,46] The δ^{202}Hg, Δ^{199}Hg, and Δ^{200}Hg values of PBM averaged at −1.07 ± 0.85, 0.37 ± 0.34, and 0.09 ± 0.05‰ in the CFPP area, respectively, and averaged at −0.71 ± 0.77, 0.11 ± 0.14, and 0.05 ± 0.06‰ in the CP area, respectively (Table S3). The δ^{202}Hg, Δ^{199}Hg, and Δ^{200}Hg values in PBM were significantly different between the CFPP and CP areas ($p < 0.05$). Additionally, the δ^{202}Hg, Δ^{199}Hg, and Δ^{200}Hg of precipitation THg averaged at −0.64 ± 0.34, 0.54 ± 0.38, and 0.14 ± 0.06‰ in the CFPP area, respectively, and averaged at −0.92 ± 0.61, 0.24 ± 0.22, and 0.13 ± 0.06‰ in the CP area, respectively (Table S4). A significant difference in Δ^{199}Hg values of precipitation THg was found between the CFPP and CP areas ($p < 0.01$).

3.2. Seasonal Variations. GEM concentrations in the study areas showed obvious seasonal variations. In the CFPP area, the GEM concentrations were notably elevated in summer with a season mean of 6.17 ± 2.34 ng m^{-3}, which were significantly higher than those in spring (3.39 ± 0.56 ng m^{-3}), autumn (2.64 ± 0.42 ng m^{-3}) and winter (3.64 ± 0.81 ng m^{-3}) ($p < 0.01$) (Figure S1a). Higher electricity demands in summer for cooling caused higher Hg emissions from the CFPP.[12] Besides, higher temperature and stronger solar radiation in summer also enhanced soil Hg^0 emissions.[47] Such a seasonal pattern was consistent with previous observations in some Chinese cities.[36,48] However, a completely different seasonal pattern was observed in the CP area, with the highest GEM concentration in winter (6.79 ± 2.43 ng m^{-3}), followed by autumn (4.93 ± 1.33 ng m^{-3}) and spring (3.33 ± 0.30 ng m^{-3}), and the lowest in summer (2.09 ± 0.45 ng m^{-3}) (Figure S1b). The decrease in GEM concentrations in spring and summer 2022 compared to those in autumn and winter 2021 was attributed to cessation or reduction of cement production in the CP area. According to the local government statistical report, cement output in 2022 has decreased by 51.6% compared to 2021 (available at https://www.longli.gov.cn/zwgk/xxgkml/jcxxgk/tjxx/tjgb/202307/t20230714_81871009.html). Additionally, the lower GEM concentration in summer in the CP area may be driven by reduction of residential coal combustion[49,50] and enhancement of vegetation photosynthesis,[36] given that most of the eastern CP area is forested (Figure 1b).

The PBM concentrations in the CFPP area in autumn were higher than those in other seasons but without statistical differences ($p > 0.05$) (Figure S1c). The PBM concentrations in the CP area were significantly higher in autumn and winter than in spring and summer ($p < 0.01$) (Figure S1d). Significantly positive correlations were indeed observed between PBM and TSP concentrations ($p < 0.01$) (Figure S2). Elevated PBM concentrations in autumn in the CFPP area may be related to biomass burning, which is indicated by a significant increase in TSP concentrations in autumn. Higher PBM concentrations in winter were also related to the temperature-dependent gas-particle partitioning between GOM and PBM, heightened anthropogenic emissions from biomass burning and residential coal combustion, and unfavorable meteorological conditions for pollutants diffusion.[14,38]

Seasonal average precipitation THg concentrations were 14.2 ± 8.15, 21.3 ± 6.02, 10.0 ± 2.92 and 14.3 ± 5.70 ng L^{-1} in spring, summer, autumn and winter, respectively, in the CFPP area (Figure S1e), and the corresponding concentrations were 9.99 ± 2.50, 7.33 ± 2.97, 15.6 ± 5.84 and 171 ± 229 ng L^{-1} in the CP area (Figure S1f). The seasonal variations of precipitation THg concentrations were partly driven by the frequency of precipitation. Annual average rainfall in two study areas follows the seasonal pattern of summer > spring > autumn > winter (China Meteorological Science Data Center, available at http://data.cma.cn). Apart from impacts of the frequency of precipitation, Hg emissions from the CP significantly elevated the precipitation THg concentrations in winter. However, precipitation THg concentration in the CFPP area was higher in summer than in the other seasons, which was associated with higher Hg emissions from the CFPP resulting from increased demands of electricity for cooling purpose. The lower precipitation THg concentrations in winter in the CFPP area may be attributed to a mixture of rain and snow, which was found in previous studies that Hg concentrations in snow samples were much lower than those in rain samples.[16,51]

The isotopic compositions of GEM, PBM and precipitation THg also displayed significant seasonal variations, although with significant differences between the two study areas. In the CFPP area, the mean $\delta^{202}Hg_{GEM}$ values in summer and winter were lower than those in spring and autumn ($p < 0.01$), as shown in Figure S3, which was consistent with the observations in several cities in China.[36] The $\Delta^{199}Hg_{GEM}$ values were near-zero in summer and winter and negative in spring and autumn. Combined with the seasonal variations of GEM concentrations, the lower $\delta^{202}Hg_{GEM}$ and elevated $\Delta^{199}Hg_{GEM}$ values in summer and winter were significantly impacted by higher coal Hg emissions. In the CP area, lower $\Delta^{199}Hg_{GEM}$ values were observed in summer than in the other seasons, which were caused by the reduction of Hg emissions with near-zero Δ^{199}Hg from the CP.

As PBM concentrations were elevated in autumn in the CFPP area, the $\delta^{202}Hg_{PBM}$ and $\Delta^{199}Hg_{PBM}$ in autumn were also different from those in the other seasons (Figure S4), with significantly higher $\Delta^{199}Hg_{PBM}$ values ranging from 0.36 to 1.54‰. The observed higher $\Delta^{199}Hg_{PBM}$ values in autumn may be impacted by PBM from long-range transport, which were comparable to those of PBM in remote areas of China.[39] In the CP area, near-zero values of $\Delta^{199}Hg_{PBM}$ in spring, autumn, and winter indicated the significant impact of near-zero Δ^{199}Hg of GOM through gas-particle partitioning and PBM emitted from cement production.[22,52] The higher $\Delta^{199}Hg_{PBM}$ values (average at 0.25‰) in summer were likely related to a decrease in Hg emissions from cement production. Besides, the enhanced photoreduction of PBM in summer under stronger solar radiation may also elevate the $\Delta^{199}Hg_{PBM}$ values.[39]

For isotopic compositions of precipitation THg (Figure S5), more positive Δ^{199}Hg values were found in winter in the CFPP area, while significantly elevated Δ^{199}Hg values were observed in summer in the CP area. The relatively positive Δ^{199}Hg in summer in the CP area was mainly caused by the enhanced GOM photoreduction under stronger solar radiation. In addition, the Δ^{200}Hg values of precipitation THg were more

https://doi.org/10.1021/acs.est.4c07649
Environ. Sci. Technol. 2024, 58, 16855−16866

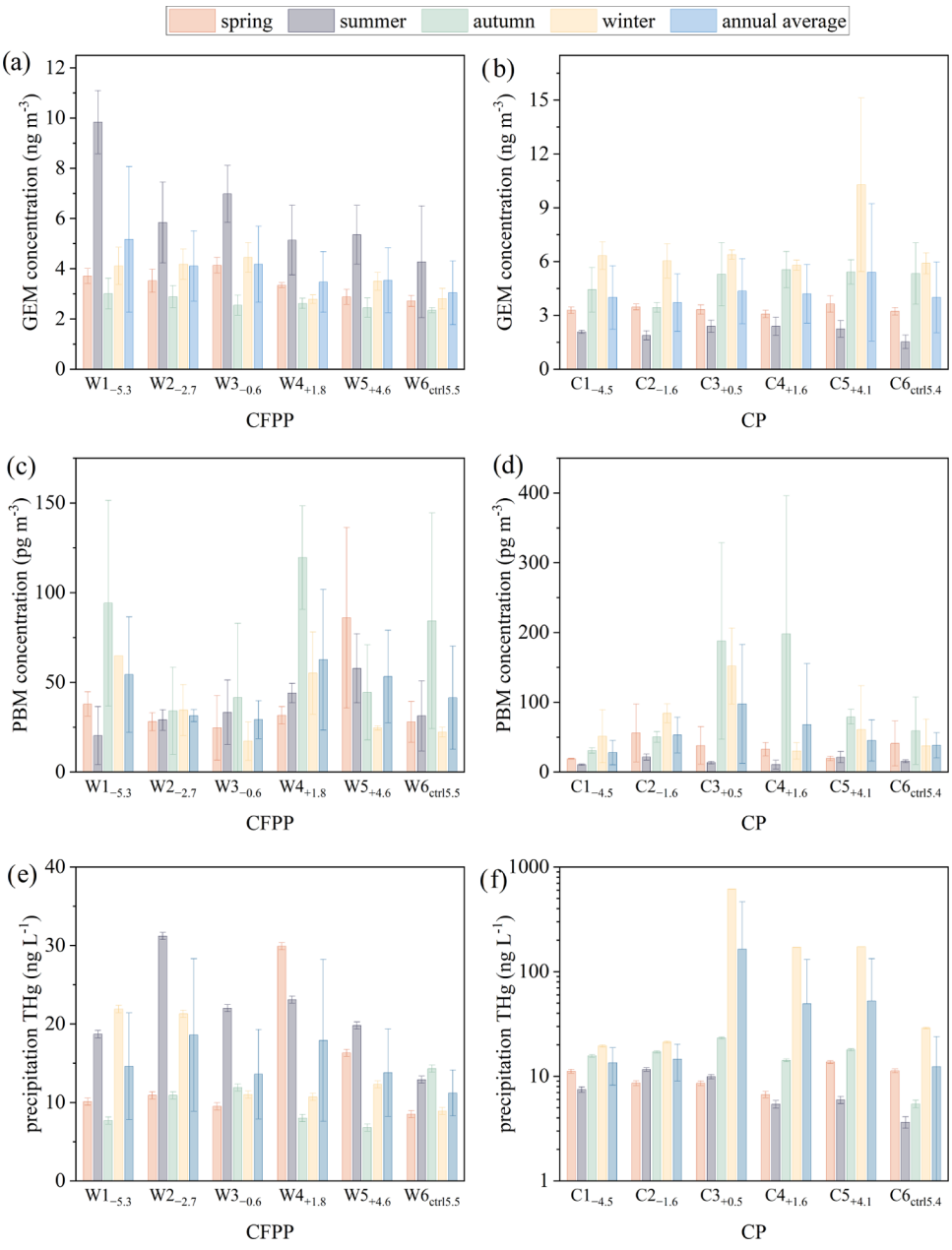

Figure 2. Spatial and seasonal variations of GEM, PBM, and precipitation THg concentrations in the CFPP area (a, c, e) and CP area (b, d, f). For the sampling point subscripts, "−" represents upwind direction, "+" represents downwind direction, and number represents the distance between sampling point and Hg source.

positive than those of GEM and PBM in both study areas due to upper tropospheric and/or stratospheric redox reactions.[16]

3.3. Spatial Variations − Implications of Emission Sources Impacts. The variations of concentrations of atmospheric GEM and PBM and precipitation THg with the distance from the CFPP or CP are shown in Figure 2. In the CFPP area, the annual average GEM concentrations at each point (W1−W6) were 5.17 ± 2.90, 4.11 ± 1.40, 4.18 ± 1.51, 3.47 ± 1.21, 3.54 ± 1.29, and 3.04 ± 1.27 ng m^{-3}, respectively (Figure 2a). The annual average was highest at point $W1_{-5.3}$ ("−" representing the upwind direction, and the number representing the distance (5.3 km) away from the source), followed by point $W3_{-0.6}$, and the lowest concentration was at the control point $W6_{ctrl,\ 5.5}$. Much higher GEM concentrations at point $W1_{-5.3}$ in summer may be related to the re-emission of Hg from the soil because soil Hg concentration near point $W1_{-5.3}$ was higher (348 ± 27.6 ng g^{-1}) than the averaged soil Hg concentration (120 ± 67.0 ng g^{-1}) at the other points. If the summer data were excluded, the highest annual average GEM concentration would appear at point $W3_{-0.6}$. Significant differences in GEM concentrations were found between the point $W3_{-0.6}$ and the two downwind points ($W4_{+1.8}$ and $W5_{+4.6}$ ("+" representing the downwind direction)), and between the point $W3_{-0.6}$ and the control point $W6_{ctrl,\ 5.5}$ ($p < 0.01$), but no significant difference was observed between the point $W3_{-0.6}$ and the two upwind points ($W1_{-5.3}$ and $W2_{-2.6}$) ($p > 0.05$).

In the CP area, the annual average GEM concentrations at points (C1−C6) were 4.00 ± 1.77, 3.71 ± 1.61, 4.35 ± 1.82, 4.20 ± 1.63, 5.40 ± 3.83, and 4.00 ± 1.98 ng m^{-3}, respectively (Figure 2b). GEM concentrations at point $C5_{+4.1}$ showed a

https://doi.org/10.1021/acs.est.4c07649
Environ. Sci. Technol. 2024, 58, 16855−16866

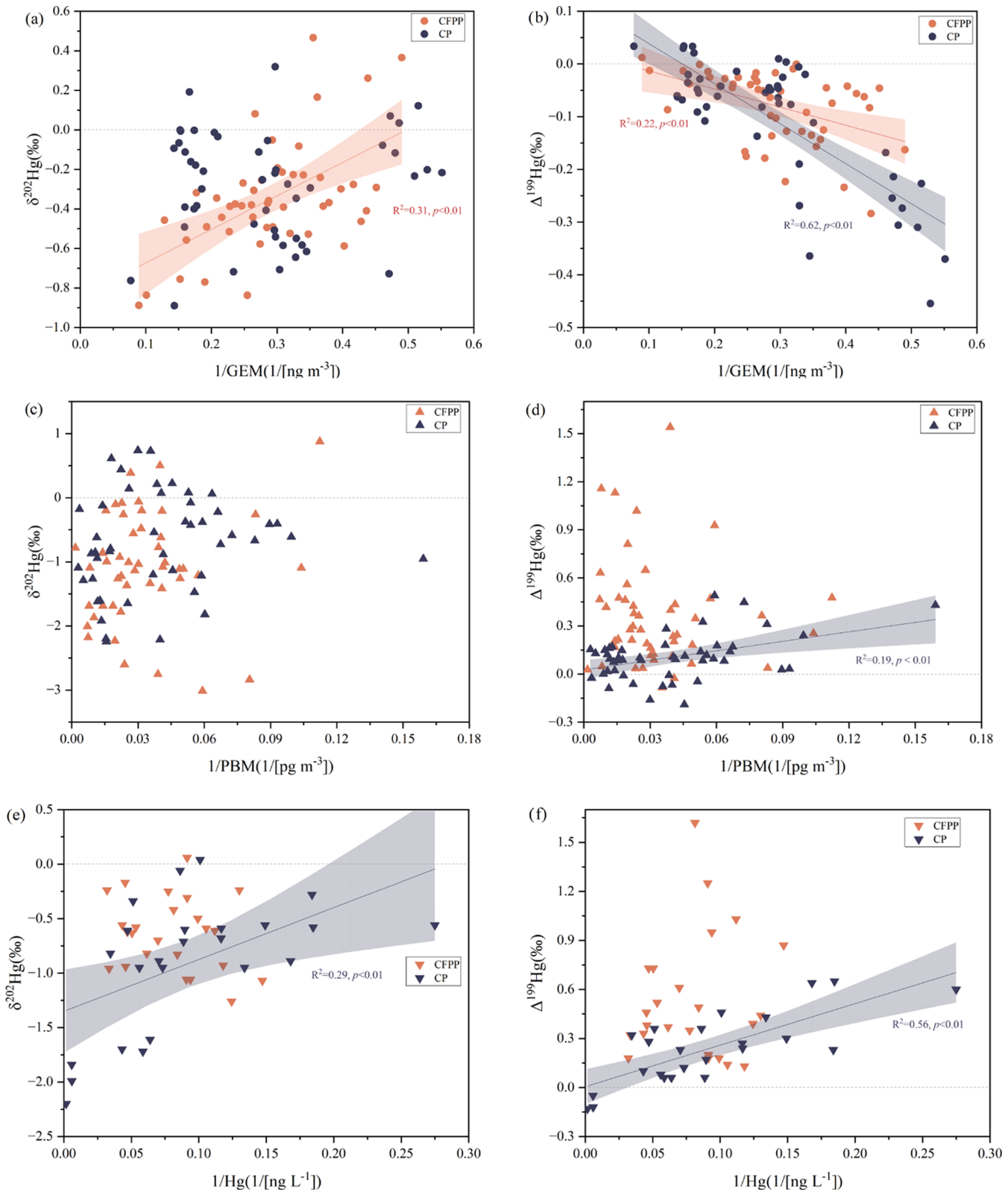

Figure 3. Linear correlations of Hg concentrations versus Hg isotopes (δ^{202}Hg and Δ^{199}Hg) in GEM (a, b), PBM (c, d), and precipitation samples (e, f).

significant difference from those at the other points ($p < 0.01$). The elevated GEM concentrations at point $C5_{+4.1}$ in winter were attributed to the increased residential Hg emissions (burning wood for warming) in nearby towns. If winter data were excluded, the highest annual average GEM concentration would appear at point $C3_{+0.5}$. No statistical differences were observed between point $C3_{+0.5}$ and the downwind points ($C4_{+1.6}$ and $C5_{+4.1}$) ($p > 0.05$). These results indicated that the impacts of Hg^0 emission from flue gas of CFPP and CP on GEM concentrations varied with distances from the plants, while the

https://doi.org/10.1021/acs.est.4c07649
Environ. Sci. Technol. 2024, 58, 16855−16866

GEM concentrations at points ($W1_{-5.3}$ and $C5_{+4.1}$), which are farther away from the plants, were also influenced by other human activities or soil Hg emissions.

The annual average PBM concentrations at points (W1−W6) in the CFPP area were 54.3 ± 32.2, 31.4 ± 3.4, 29.2 ± 10.6, 62.6 ± 39.2, 53.2 ± 25.8, and 41.4 ± 28.8 pg m^{-3}, respectively (Figure 2c). The PBM concentrations at downwind points ($W4_{+1.8}$ and $W5_{+4.6}$) were slightly higher than those at upwind points ($W2_{-2.7}$ and $W3_{-0.6}$) and point $W6_{ctrl,5.5}$ in the CFPP area but without statistically significant difference ($p > 0.05$). In the CP area, annual average PBM concentrations at points (C1−C6) were 27.8 ± 17.6, 53.0 ± 25.6, 97.8 ± 85.1, 68.0 ± 87.4, 45.2 ± 29.6, and 38.3 ± 18.0 pg m^{-3}, respectively (Figure 2d). The PBM concentration at point $C3_{+0.5}$ was significantly elevated compared to that at upwind points ($C1_{-4.5}$ and $C2_{-1.6}$) ($p < 0.01$). The annual average PBM concentration was the highest near the source and gradually decreased with increasing distance. Although the proportion of PBM out of total emitted Hg from flue gas was less than 1% generally,[43] PBM can be formed from GOM through gas-particle partitioning; thus, flue gas with a high proportion of divalent Hg emitted from the CP would significantly increase the PBM concentrations.

Annual average precipitation THg concentrations in the CFPP area at points W1 to W6 varied from 11.2 to 18.6 ng L^{-1}, with an average of 14.9 ng L^{-1}. The differences in precipitation THg concentration were not statistically significant between the sampling points ($p > 0.05$). Annual average precipitation THg concentrations in the CP area were 13.4 ± 5.24, 14.6 ± 5.63, and 12.3 ± 11.6 ng L^{-1} at upwind point $C1_{-4.5}$ and $C2_{-1.6}$, and control point $C6_{ctrl,5.4}$, respectively, and median precipitation THg concentrations were 16.6 (interquartile range (IQR): 8.90−467), 15.8 (IQR: 7.88−134), and 10.4 (IQR: 5.73−132) ng L^{-1} at downwind point $C3_{+0.5}$, $C4_{+1.6}$, and $C5_{+4.1}$, respectively (Figure 2f). Precipitation THg concentrations in winter were significantly elevated at point $C3_{+0.5}$ (615.6 ng L^{-1}) and sharply decreased by about 72% at downwind points ($C4_{+1.6}$ and $C5_{+4.1}$). Significant spatial variations of PBM and precipitation THg concentrations in the CP area were due to a higher proportion of Hg^{II} in the flue gas of cement production. Despite the installation of air pollution control devices (APCDs) that have significantly reduced Hg emissions from coal combustion and cement production, elevated atmospheric Hg concentrations were still observed in areas close to these point sources.

GEM isotopic compositions in the study areas are displayed in Figure S6. Significant differences in $\delta^{202}Hg_{GEM}$ were identified between upwind points ($W1_{-5.3}$ and $W2_{-2.7}$) and one downwind point ($W4_{+1.8}$) in summer and autumn in the CFPP area ($p < 0.01$). In the CP area, $\delta^{202}Hg_{GEM}$ gradually decreased in the prevailing wind direction (from point $C1_{-4.5}$ to point $C5_{+4.1}$). $\delta^{202}Hg_{GEM}$ values were slightly positive in background air[15] and negative for anthropogenic emissions,[22,52] and thus the negative $\delta^{202}Hg_{GEM}$ at the downwind sampling points were likely affected by cement production. In the CP area, summertime $\Delta^{199}Hg_{GEM}$ values were the highest at point $C3_{+0.5}$, influenced by near-zero $\Delta^{199}Hg$ values of flue gas emissions from the CP, and then gradually decreased with an increasing distance.

Correlations between atmospheric Hg concentrations and Hg isotopic compositions have been widely used to trace potential Hg sources and the transformation process in the atmosphere.[44,45] A positive correlation was found between $\delta^{202}Hg_{GEM}$ and $1/GEM_{conc.}$ in the CFPP area with an intercept of −0.84 ± 0.11‰ (Figure 3), indicating that flue gas Hg emissions from the CFPP have an impact on ambient GEM, but no significant relationship was found in the CP area. The $\Delta^{199}Hg_{GEM}$ negatively correlated with $1/GEM_{conc.}$, with the intercepts being 0.02 ± 0.03 and 0.11 ± 0.03‰ in the CFPP and CP area, respectively, which are comparable to the estimated mean value (−0.05 ± 0.06‰) of global coal Hg emissions[53] and stack gas of cement production (0.10 ± 0.02‰).[52] The ratios of $\Delta^{199}Hg/\Delta^{201}Hg$ were 0.92 and 1.10 in the CFPP and CP area, respectively (Figure S7a). These results indicated that photochemical reduction of Hg^{II} was the dominant reaction to drive the odd-MIF variation of GEM.

Due to the low emissions of PBM from anthropogenic sources under the control of APCDs, the spatial variations of PBM isotopes were not significant (Figure S8). However, $\Delta^{199}Hg_{PBM}$ and $\Delta^{200}Hg_{PBM}$ in the CP area were significantly lower than those in the CFPP area ($p < 0.05$), indicating a stronger impact of atmospheric Hg emitted from the CP on local particles. No significant correlations were identified between $\delta^{202}Hg_{PBM}$ and $1/PBM_{conc.}$ in the two study areas. A significant positive correlation was observed between $\Delta^{199}Hg_{PBM}$ and $1/PBM_{conc.}$ in the CP area ($p < 0.01$), with an intercept of 0.03 ± 0.03‰ (Figure 3d), which was consistent with that of PBM emitted from cement production.[52] The $\Delta^{199}Hg$ values increased with decreasing PBM concentrations in the CP area, indicating the impact of emission sources on PBM mainly occurred on a local scale. The $\Delta^{199}Hg/\Delta^{201}Hg$ ratios of the PBM were 1.57 and 1.08 in the CFPP and CP area, respectively (Figure S7b). The $\Delta^{199}Hg/\Delta^{201}Hg$ ratio in the CFPP area was different from that of world coal[53,54] and other anthropogenic sources,[18] which generally have a small magnitude of odd-MIF and a $\Delta^{199}Hg/\Delta^{201}Hg$ ratio of ∼1.0. Excluding data points in autumn would result in a ratio of 1.32, which was adjacent to the slope (1.0−1.3) generated by photoreduction of Hg^{II}.[35] The MIF induced by the nuclear volume effect (NVE) shows a $\Delta^{199}Hg/\Delta^{201}Hg$ ratio of ∼1.6; however, negative $\Delta^{199}Hg$ signatures were generated in reactant Hg^{II}.[55] Thus, the higher $\Delta^{199}Hg/\Delta^{201}Hg$ ratio of PBM was considered to be induced by not only photoreduction of Hg^{II} but also other in-aerosol heterogeneous Hg reactions.[14]

There were generally no statistical differences in the isotopes of precipitation THg between different sites in both study areas (Figure S9). One exception is winter precipitation samples in the CP area, which showed significantly different isotopes from the other samples. The winter samples showed negative $\Delta^{199}Hg$ values and near-zero $\Delta^{200}Hg$ values, which were consistent with the previously reported GOM isotopic compositions of flue gas.[52] Moreover, $\delta^{202}Hg$ and $\Delta^{199}Hg$ of precipitation THg showed a significant correlation with $1/Hg_{conc.}$ in the CP area but not in the CFPP area (Figure 3e,f) due to the significantly different Hg speciation profiles in flue gas emissions between the two plants. This demonstrated that the high proportion of divalent Hg in flue gas emitted from CP generated a great influence on Hg isotopic compositions in local wet deposition.

3.4. Source Apportionment. The discussion mentioned above shows that the concentrations and isotopic compositions of ambient GEM and PBM around the CFPP and CP varied in seasonality and spatiality. Such variations were affected by not only Hg point source emissions but also local environmental conditions. The surface soil Hg emission was also a noteworthy source, especially in summer. Therefore, we first clarify the isotope characteristics of potential Hg sources and then calculate the average relative contributions of the dominant Hg sources for GEM and PBM samples.

https://doi.org/10.1021/acs.est.4c07649
Environ. Sci. Technol. 2024, 58, 16855−16866

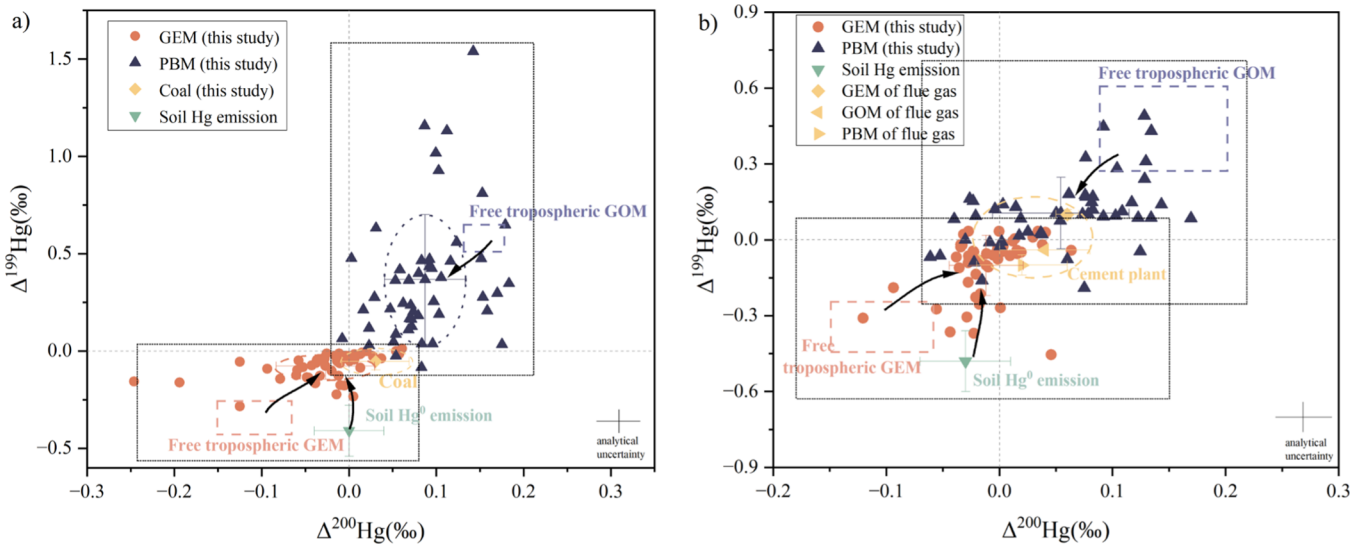

Figure 4. Plots of Δ^{200}Hg versus Δ^{199}Hg used to source apportionment of GEM and PBM samples in the CFPP area (a) and CP area (b). The orange and dark purple rectangles represent variation ranges of Hg isotope compositions of background-free tropospheric GEM pool[19,25,66] and background-free tropospheric GOM pool,[19] respectively. The Δ^{199}Hg values of soil Hg^0 emissions were calculated by equation: $E^{199}Hg_{soil\ emission} = \Delta^{199}Hg_{soil\ Hg(0)\ exchange} - \Delta^{199}Hg_{soil} = -0.0007SR - 0.005$,[64] and Δ^{200}Hg values are represented by those of soil.

The potential Hg sources of GEM in the study areas included anthropogenic emissions (i.e., GEM from flue gas), land surface emissions, and intrusion from background free tropospheric GEM pool.[15] According to model simulations and field experiments reported in earlier studies, the Δ^{199}Hg and Δ^{200}Hg values of flue gas Hg emitted from CFPP and CP were consistent with those of the raw materials.[22,53,56−58] Therefore, the Δ^{199}Hg and Δ^{200}Hg values of anthropogenic source emissions in the CFPP and CP areas can be represented by those of feed coal and raw materials. Previous studies reported that in-plume Hg^{II} emitted from CFPPs might be rapidly reduced to Hg^0,[59,60] but field observations suggested that differences between in-stack and in-plume Hg^{II} concentrations were owing to sampling biases of different measurement techniques.[61] Moreover, aircraft observations[62] and anthropogenic Hg emission inventories[63] suggested that previously reported in-plume Hg^{II} reduction may be attributed to an overestimation of Hg^{II} emissions in flue gas.[64] Thus, we assumed that rapid in-plume Hg^{II} reduction was negligible. The Hg concentration of feed coal collected in the CFPP was 147 ± 33.8 ng g^{-1} (n = 4), and δ^{202}Hg, Δ^{199}Hg and Δ^{200}Hg values were −1.09 ± 0.12, −0.05 ± 0.04 and 0.03 ± 0.04‰, respectively (Table S3). The Hg concentration and isotopes of flue gas in the CP have been reported in a previous study, as shown in Table S6.[52] The Hg concentrations and isotopes of surface soil near sampling points were measured and are shown in Table S5. Given that Δ^{199}Hg values of Hg^0 emitted from soil were impacted by Δ^{199}Hg of soil and solar radiation (SR), the Δ^{199}Hg values of land surface emissions in the study areas were recalculated based on soil Δ^{199}Hg values and SR during the sampling periods, i.e., $E^{199}Hg_{soil\ emission} = \Delta^{199}Hg_{soil\ Hg(0)\ exchange} - \Delta^{199}Hg_{soil} = -0.0007SR - 0.005$, and details are showed in Table S5.[65] The process of Hg^0 emitted from soil would not yield significant even-MIF.[65] Therefore, the Δ^{200}Hg values of land surface emissions were represented by those of soils.

The binary/ternary mixed model of Hg isotopes has been widely used to trace the sources of atmospheric Hg. The δ^{202}Hg can be largely shifted by both biotic and abiotic processes; therefore, it was not used in the mixed model. Although Δ^{199}Hg and Δ^{200}Hg of GEM may be changed by photoredox processes, they are not expected to be converted significantly on local to regional scales during short time periods because of very low atmospheric Hg^0 photoredox rates in the continental boundary layer.[64,66] Therefore, we used a ternary mixture model of Δ^{199}Hg and Δ^{200}Hg to identify the relative contributions of different sources to atmospheric GEM (eqs 3−5).

$$\Delta^{199}Hg_{sample} = F_{(anthropogenic)} \times \Delta^{199}Hg_{(anthropogenic)} + F_{(land\ surface)} \times \Delta^{199}Hg_{(surface)} + F_{(background)} \times \Delta^{199}Hg_{(background)} \quad (3)$$

$$\Delta^{200}Hg_{sample} = F_{(anthropogenic)} \times \Delta^{200}Hg_{(anthropogenic)} + F_{(land\ surface)} \times \Delta^{200}Hg_{(surface)} + F_{(background)} \times \Delta^{200}Hg_{(background)} \quad (4)$$

$$1 = F_{(anthropogenic)} + F_{(land\ surface)} + F_{(background)} \quad (5)$$

where $F_{(anthropogenic)}$, $F_{(land\ surface)}$, and $F_{(background)}$ are the fractions of surface GEM sourced from anthropogenic emissions, land surface emissions, and background-free tropospheric pool, respectively; $\Delta^{199}Hg_{sample}$ and $\Delta^{200}Hg_{sample}$ are the measured MIF values of GEM samples; and $\Delta^{199}Hg_{anthropogenic}$ and $\Delta^{200}Hg_{anthropogenic}$ are the MIF signatures of anthropogenic emissions measured in the CFPP or CP area.

In the CFPP area (Figure 4a), the end member values of Δ^{199}Hg and Δ^{200}Hg were identified for the feed coal (Δ^{199}Hg: −0.05 ± 0.04‰; Δ^{200}Hg: 0.03 ± 0.04‰), land surface emissions (Δ^{199}Hg: −0.41 ± 0.13‰; Δ^{200}Hg: 0.00 ± 0.04‰) and background free tropospheric GEM pool (Δ^{199}Hg: −0.33 ± 0.07‰; Δ^{200}Hg: −0.10 ± 0.02‰) (Table S6).[19,25,67] The average relative contributions to GEM from these three sources were then estimated to be 58.3 ± 20.9, 16.0 ± 14.6, and 25.7 ± 19.5%, respectively. Similarly, in the CP area (Figure 4b), the end member values were assigned to anthropogenic emissions, i.e., GEM of flue gas of CP (Δ^{199}Hg: 0.10 ± 0.02‰; Δ^{200}Hg:

https://doi.org/10.1021/acs.est.4c07649
Environ. Sci. Technol. 2024, 58, 16855−16866

0.06 ± 0.01‰),[52] land surface emissions (Δ^{199}Hg: −0.48 ± 0.12‰; Δ^{200}Hg: −0.03 ± 0.04‰), and background (Δ^{199}Hg: −0.33 ± 0.07‰; Δ^{200}Hg: −0.10 ± 0.02‰)[19,25,67] (Table S6). The average relative contributions to GEM from these three sources were estimated to be 47.0 ± 16.7, 24.2 ± 17.4, and 28.8 ± 16.7%, respectively.

The sources of PBM were very complex, including direct emissions from anthropogenic sources, gas-particle partitioning of GOM emitted from anthropogenic sources, and oxidation of GEM, followed by gas-particle partitioning of GOM. PBM and GOM emitted from CP inherited the MIF values from raw materials.[22] Shift of even-MIF (Δ^{200}Hg) only induced by photochemical Hg redox reactions in specific environments, such as in the upper stratosphere or at high altitudes.[19,68] The odd-MIF (Δ^{199}Hg) of PBM, however, could be shifted significantly through regional-scale atmospheric transport from anthropogenic sources.[14,39,69] Hence, we used a binary mixed model of Hg isotopes based on Δ^{200}Hg to estimate the relative contributions of different sources to the PBM.

$$\Delta^{200}\mathrm{Hg}_{\mathrm{sample}} = F_{(\mathrm{anthropogenic})} \times \Delta^{200}\mathrm{Hg}_{(\mathrm{anthropogenic})} + F_{(\mathrm{background})} \times \Delta^{200}\mathrm{Hg}_{(\mathrm{background})} \quad (6)$$

$$1 = F_{(\mathrm{anthropogenic})} + F_{(\mathrm{background})} \quad (7)$$

The Δ^{200}Hg signature of GOM produced in the free troposphere ($\Delta^{200}\mathrm{Hg}_{\mathrm{background}}$) was estimated to be 0.15 ± 0.06‰ (Table S6).[14,19] The end member value of Δ^{200}Hg of PBM for the anthropogenic sources (i.e., feed coal) in the CFPP area was 0.03 ± 0.04‰.[28] The average relative contributions to PBM in the CFPP area were estimated to be 52.3 ± 25.9% from anthropogenic emissions and 47.7 ± 25.9% from the background, on average. Similarly, the end member value of Δ^{200}Hg for the anthropogenic sources (i.e., Δ^{200}Hg of PBM and GOM emitted from cement production) was 0.03 ± 0.04‰.[52] The average relative contributions to PBM in the CP area were estimated to be 60.0 ± 25.9% from anthropogenic emissions and 40.0 ± 25.9% from the background.

The contributions of CFPP and CP to local GEM and PBM showed seasonal variations, as shown in Figure S10. The higher contribution of CFPP to GEM in summer demonstrated that the higher electricity demands in summer, and higher contribution to PBM in winter was related to the local environmental conditions. In the CP area, the contributions of CP to GEM and PBM were lower in summer, which was consistent with the seasonal variations of GEM and PBM concentrations owing to decreased cement output. Moreover, contributions of the CFPP and CP to ambient GEM in the study areas had weak spatial variation trends, with the highest contributions of the CFPP and CP appearing at points $W4_{+1.8}$ and $C3_{+0.4}$ in the prevailing downwind direction, respectively (Figure S11). Contributions of the CFPP to ambient PBM in the CFPP area also showed weak spatial variation in the prevailing downwind direction. There was no spatial variation trend for contributions of CP to PBM in the CP area. However, the overall impact of Hg emissions on the PBM in the CP area was higher than that in the CFPP area.

The source apportionment analysis results presented above suggested that atmospheric Hg emissions from the CFPP mainly impacted ambient GEM, while those from the CP impacted more on PBM and precipitation THg due to the higher proportions of flue gas GOM emissions.

4. ENVIRONMENTAL IMPLICATIONS

Characterizing atmospheric Hg emissions from source sectors and their impacts on local to regional atmospheric Hg transport and deposition is crucial for the effectiveness evaluation of the implementation of the Minamata Convention on Mercury. Seasonal and spatial variations in Hg concentrations and isotopes revealed that GEM and PBM were affected by not only Hg point source emissions but also local meteorological conditions. In addition, the surface soil Hg emission was also an important source of local atmospheric Hg. Although a large portion of Hg emitted from anthropogenic emissions can be captured by APCDs, the remaining portion of atmospheric Hg emissions from these sources can still have significant effects on natural environment, especially at local to regional scales. Moreover, Hg speciation has significant impacts on its transport distance. The increasing use of new suspension preheater/precalciner (NSP) kilns, replacing shaft kilns and other rotary kilns, is expected to reduce the synergistic Hg removal efficiency of APCDs,[11,70] leading to a significant increase in the Hg^{II} emissions from cement production. Source apportionment analysis based on Hg isotopes provided evidence that the increase in cement-related Hg^{II} emissions would enhance local Hg deposition,[11] which would have important implications on the ecosystem and human health because newly deposited Hg is more easily to be methylated to toxic MeHg. Therefore, reduction of speciated Hg emissions for the effectiveness evaluation of convention should be considered. Quantification of the local- to regional-scale deposition of speciated atmospheric Hg in areas with anthropogenic Hg emissions is of great importance for assessing soil Hg accumulation and subsequent methylation in various ecosystems in order to minimize the Hg exposure risks.

■ ASSOCIATED CONTENT

Supporting Information

The Supporting Information is available free of charge at https://pubs.acs.org/doi/10.1021/acs.est.4c07649.

Additional information about Hg isotope signals of standards, the data sets of Hg concentrations and isotope compositions in GEM, PBM, precipitation, soil and potential source endmembers, and 11 supplemental figures, including seasonal and spatial variation of Hg concentrations and isotope compositions in GEM, PBM, and precipitation and estimated contributions of potential sources to GEM and PBM. (PDF)

■ AUTHOR INFORMATION

Corresponding Author

Ping Li − *State Key Laboratory of Environmental Geochemistry, Institute of Geochemistry, Chinese Academy of Sciences, Guiyang 550081, China;* orcid.org/0000-0002-0145-4122; Phone: +86 851 84391375; Email: liping@mail.gyig.ac.cn; Fax: +86 851 85891609

Authors

Chuan Wang − *State Key Laboratory of Environmental Geochemistry, Institute of Geochemistry, Chinese Academy of Sciences, Guiyang 550081, China; University of Chinese Academy of Sciences, Beijing 100049, China*

Shaochen Yang − *State Key Laboratory of Environmental Geochemistry, Institute of Geochemistry, Chinese Academy of Sciences, Guiyang 550081, China*

https://doi.org/10.1021/acs.est.4c07649
Environ. Sci. Technol. 2024, 58, 16855−16866

Ruolan Li − *State Key Laboratory of Environmental Geochemistry, Institute of Geochemistry, Chinese Academy of Sciences, Guiyang 550081, China; University of Chinese Academy of Sciences, Beijing 100049, China*
Junyao Yan − *State Key Laboratory of Environmental Geochemistry, Institute of Geochemistry, Chinese Academy of Sciences, Guiyang 550081, China*
Yanxin Hu − *State Key Laboratory of Environmental Geochemistry, Institute of Geochemistry, Chinese Academy of Sciences, Guiyang 550081, China*
Chuyan Lai − *State Key Laboratory of Environmental Geochemistry, Institute of Geochemistry, Chinese Academy of Sciences, Guiyang 550081, China; University of Chinese Academy of Sciences, Beijing 100049, China*
Zhonggen Li − *College of Resources and Environment, Zunyi Normal University, Zunyi 563006, China;* orcid.org/0000-0001-7400-6294
Leiming Zhang − *Air Quality Research Division, Science and Technology Branch, Environment and Climate Change Canada, Toronto, Ontario M3H 5T4, Canada;* orcid.org/0000-0001-5437-5412
Xinbin Feng − *State Key Laboratory of Environmental Geochemistry, Institute of Geochemistry, Chinese Academy of Sciences, Guiyang 550081, China; University of Chinese Academy of Sciences, Beijing 100049, China;* orcid.org/0000-0002-7462-8998

Complete contact information is available at: https://pubs.acs.org/10.1021/acs.est.4c07649

Notes

The authors declare no competing financial interest.

■ ACKNOWLEDGMENTS

This study was funded by National Natural Science Foundation of China (42077315), the CAS Interdisciplinary Innovation Team (JCTD-2020-20), Youth Innovation Promotion Association of Chinese Academy of Sciences (Y2021106), and Guizhou Provincial 2020 Science and Technology Subsidies (No. GZ2020SIG).

■ REFERENCES

(1) Ariya, P. A.; Amyot, M.; Dastoor, A.; Deeds, D.; Feinberg, A.; Kos, G.; Poulain, A.; Ryjkov, A.; Semeniuk, K.; Subir, M.; Toyota, K. Mercury physicochemical and biogeochemical transformation in the atmosphere and at atmospheric interfaces: a review and future directions. *Chem. Rev.* **2015**, *115* (10), 3760−3802.
(2) Gustin, M.; Jaffe, D. Reducing the Uncertainty in Measurement and Understanding of Mercury in the Atmosphere. *Environ. Sci. Technol.* **2010**, *44* (7), 2222−2227.
(3) Wu, Q.; Wang, S.; Li, G.; Liang, S.; Lin, C. J.; Wang, Y.; Cai, S.; Liu, K.; Hao, J. Temporal Trend and Spatial Distribution of Speciated Atmospheric Mercury Emissions in China During 1978−2014. *Environ. Sci. Technol.* **2016**, *50* (24), 13428−13435.
(4) Zhang, L.; Wang, S.; Wu, Q.; Wang, F.; Lin, C.-J.; Zhang, L.; Hui, M.; Yang, M.; Su, H.; Hao, J. Mercury transformation and speciation in flue gases from anthropogenic emission sources: a critical review. *Atmos. Chem. Phys.* **2016**, *16* (4), 2417−2433.
(5) Zhang, Y.; Zhang, L.; Cao, S.; Liu, X.; Jin, J.; Zhao, Y. Improved Anthropogenic Mercury Emission Inventories for China from 1980 to 2020: Toward More Accurate Effectiveness Evaluation for the Minamata Convention. *Environ. Sci. Technol.* **2023**, *57* (23), 8660−8670.
(6) Zhang, L.; Wright, L. P.; Blanchard, P. A review of current knowledge concerning dry deposition of atmospheric mercury. *Atmos. Environ.* **2009**, *43* (37), 5853−5864.
(7) Wright, L. P.; Zhang, L.; Cheng, I.; Aherne, J.; Wentworth, G. R. Impacts and Effects Indicators of Atmospheric Deposition of Major Pollutants to Various Ecosystems - A Review. *Aerosol Air Qual. Res.* **2018**, *18* (8), 1953−1992.
(8) Tian, L.; Guan, W.; Ji, Y.; He, X.; Chen, W.; Alvarez, P. J. J.; Zhang, T. Microbial methylation potential of mercury sulfide particles dictated by surface structure. *Nat. Geosci.* **2021**, *14* (6), 409−416.
(9) UN-Environment. *Global Mercury Assessment*, 2018.
(10) Zhang, L.; Wang, S.; Wang, L.; Wu, Y.; Duan, L.; Wu, Q.; Wang, F.; Yang, M.; Yang, H.; Hao, J.; Liu, X. Updated emission inventories for speciated atmospheric mercury from anthropogenic sources in China. *Environ. Sci. Technol.* **2015**, *49* (5), 3185−3194.
(11) Chen, L.; Liang, S.; Zhang, H.; Cai, X.; Chen, Y.; Liu, M.; Lin, H.; Li, Y.; Qi, J.; Tong, Y.; Zhang, W.; Wang, X.; Shu, J. Rapid Increase in Cement-Related Mercury Emissions and Deposition in China during 2005−2015. *Environ. Sci. Technol.* **2020**, *54* (22), 14204−14214.
(12) Liu, K.; Wang, S.; Wu, Q.; Wang, L.; Ma, Q.; Zhang, L.; Li, G.; Tian, H.; Duan, L.; Hao, J. A Highly Resolved Mercury Emission Inventory of Chinese Coal-Fired Power Plants. *Environ. Sci. Technol.* **2018**, *52* (4), 2400−2408.
(13) Han, D.; Wu, Q.; Wen, M.; Tang, Y.; Li, G.; Ren, Y.; Cui, Y.; Li, Z.; Shi, J.; Zhang, Q.; Yin, X.; Wang, S. Isotopic Fractionation Characteristics of Speciated Mercury from Local Biomass Combustion in the Tibetan Plateau. *Environ. Sci. Technol.* **2023**, *57* (12), 4775−4783.
(14) Liu, C.; Fu, X.; Xu, Y.; Zhang, H.; Wu, X.; Sommar, J.; Zhang, L.; Wang, X.; Feng, X. Sources and Transformation Mechanisms of Atmospheric Particulate Bound Mercury Revealed by Mercury Stable Isotopes. *Environ. Sci. Technol.* **2022**, *56* (8), 5224−5233.
(15) Wu, X.; Fu, X.; Zhang, H.; Tang, K.; Wang, X.; Zhang, H.; Deng, Q.; Zhang, L.; Liu, K.; Wu, Q.; Wang, S.; Feng, X. Changes in Atmospheric Gaseous Elemental Mercury Concentrations and Isotopic Compositions at Mt. Changbai During 2015−2021 and Mt. Ailao During 2017−2021 in China. *J. Geophys. Res.* **2023**, *128* (10), No. e2022JD037749, DOI: 10.1029/2022jd037749.
(16) Yuan, S.; Chen, J.; Hintelmann, H.; Cai, H.; Yuan, W.; He, S.; Zhang, K.; Zhang, Y.; Liu, Y. Event-Based Atmospheric Precipitation Uncovers Significant Even and Odd Hg Isotope Anomalies Associated with the Circumpolar Vortex. *Environ. Sci. Technol.* **2022**, *56* (17), 12713−12722.
(17) Blum, J. D.; Sherman, L. S.; Johnson, M. W. Mercury Isotopes in Earth and Environmental Sciences. *Annu. Rev. Earth Planet. Sci.* **2014**, *42* (1), 249−269.
(18) Kwon, S. Y.; Blum, J. D.; Yin, R.; Tsui, M. T.-K.; Yang, Y. H.; Choi, J. W. Mercury stable isotopes for monitoring the effectiveness of the Minamata Convention on Mercury. *Earth-Sci. Rev.* **2020**, *203*, 103111.
(19) Fu, X.; Jiskra, M.; Yang, X.; Marusczak, N.; Enrico, M.; Chmeleff, J.; Heimburger-Boavida, L. E.; Gheusi, F.; Sonke, J. E. Mass-Independent Fractionation of Even and Odd Mercury Isotopes during Atmospheric Mercury Redox Reactions. *Environ. Sci. Technol.* **2021**, *55* (14), 10164−10174.
(20) Li, X.; Li, Z.; Chen, J.; Zhang, L.; Yin, R.; Sun, G.; Meng, B.; Cui, Z.; Feng, X. Isotope signatures of atmospheric mercury emitted from residential coal combustion. *Atmos. Environ.* **2021**, *246*, 118175.
(21) Tang, S.; Feng, C.; Feng, X.; Zhu, J.; Sun, R.; Fan, H.; Wang, L.; Li, R.; Mao, T.; Zhou, T. Stable isotope composition of mercury forms in flue gases from a typical coal-fired power plant, Inner Mongolia, northern China. *J. Hazard. Mater.* **2017**, *328*, 90−97.
(22) Li, X.; Chen, J.; Tang, L.; Wu, T.; Fu, C.; Li, Z.; Sun, G.; Zhao, H.; Zhang, L.; Li, Q.; Feng, X. Mercury isotope signatures of a pre-calciner cement plant in Southwest China. *J. Hazard. Mater.* **2021**, *401*, No. 123384.
(23) Sun, R.; Hintelmann, H.; Wiklund, J. A.; Evans, M. S.; Muir, D.; Kirk, J. L. Mercury Isotope Variations in Lake Sediment Cores in Response to Direct Mercury Emissions from Non-Ferrous Metal

Smelters and Legacy Mercury Remobilization. *Environ. Sci. Technol.* **2022**, *56* (12), 8266−8277.
(24) Yu, B.; Fu, X.; Yin, R.; Zhang, H.; Wang, X.; Lin, C. J.; Wu, C.; Zhang, Y.; He, N.; Fu, P.; Wang, Z.; Shang, L.; Sommar, J.; Sonke, J. E.; Maurice, L.; Guinot, B.; Feng, X. Isotopic Composition of Atmospheric Mercury in China: New Evidence for Sources and Transformation Processes in Air and in Vegetation. *Environ. Sci. Technol.* **2016**, *50* (17), 9262−9269.
(25) Kurz, A. Y.; Blum, J. D.; Gratz, L. E.; Jaffe, D. A. Contrasting Controls on the Diel Isotopic Variation of Hg(0) at Two High Elevation Sites in the Western United States. *Environ. Sci. Technol.* **2020**, *54* (17), 10502−10513.
(26) Huang, S.; Sun, L.; Zhou, T.; Yuan, D.; Du, B.; Sun, X. Natural stable isotopic compositions of mercury in aerosols and wet precipitations around a coal-fired power plant in Xiamen, southeast China. *Atmos. Environ.* **2018**, *173*, 72−80.
(27) Sherman, L. S.; Blum, J. D.; Keeler, G. J.; Demers, J. D.; Dvonch, J. T. Investigation of local mercury deposition from a coal-fired power plant using mercury isotopes. *Environ. Sci. Technol.* **2012**, *46* (1), 382−390.
(28) Song, Z.; Wang, C.; Ding, L.; Chen, M.; Hu, Y.; Li, P.; Zhang, L.; Feng, X. Soil mercury pollution caused by typical anthropogenic sources in China: Evidence from stable mercury isotope measurement and receptor model analysis. *J. Cleaner Prod.* **2021**, *288*, 125687.
(29) Fu, X.; Heimbürger, L.-E.; Sonke, J. E. Collection of atmospheric gaseous mercury for stable isotope analysis using iodine- and chlorine-impregnated activated carbon traps. *J. Anal. At. Spectrom.* **2014**, *29* (5), 841.
(30) Huang, Q.; Chen, J.; Huang, W.; Fu, P.; Guinot, B.; Feng, X.; Shang, L.; Wang, Z.; Wang, Z.; Yuan, S.; Cai, H.; Wei, L.; Yu, B. Isotopic composition for source identification of mercury in atmospheric fine particles. *Atmos. Chem. Phys.* **2016**, *16* (18), 11773−11786.
(31) Yan, J.; Li, R.; Ali, M. U.; Wang, C.; Wang, B.; Jin, X.; Shao, M.; Li, P.; Zhang, L.; Feng, X. Mercury migration to surface water from remediated mine waste and impacts of rainfall in a karst area − Evidence from Hg isotopes. *Water Res.* **2023**, *230*, 119592.
(32) Li, K.; Lin, C.-J.; Yuan, W.; Sun, G.; Fu, X.; Feng, X. An improved method for recovering and preconcentrating mercury in natural water samples for stable isotope analysis. *J. Anal. At. Spectrom.* **2019**, *34* (11), 2303−2313.
(33) Sun, R.; Enrico, M.; Heimburger, L. E.; Scott, C.; Sonke, J. E. A double-stage tube furnace–acid-trapping protocol for the pre-concentration of mercury from solid samples for isotopic analysis. *Anal. Bioanal. Chem.* **2013**, *405* (21), 6771−6781.
(34) Yin, R.; Krabbenhoft, D. P.; Bergquist, B. A.; Zheng, W.; Lepak, R. F.; Hurley, J. P. Effects of mercury and thallium concentrations on high precision determination of mercury isotopic composition by Neptune Plus multiple collector inductively coupled plasma mass spectrometry. *J. Anal. At. Spectrom.* **2016**, *31* (10), 2060−2068.
(35) Zhang, K.; Zheng, W.; Sun, R.; He, S.; Shuai, W.; Fan, X.; Yuan, S.; Fu, P.; Deng, J.; Li, X.; Wang, S.; Chen, J. Stable Isotopes Reveal Photoreduction of Particle-Bound Mercury Driven by Water-Soluble Organic Carbon during Severe Haze. *Environ. Sci. Technol.* **2022**, *56* (15), 10619−10628.
(36) Fu, X.; Liu, C.; Zhang, H.; Xu, Y.; Zhang, H.; Li, J.; Lyu, X.; Zhang, G.; Guo, H.; Wang, X.; Zhang, L.; Feng, X. Isotopic compositions of atmospheric total gaseous mercury in 10 Chinese cities and implications for land surface emissions. *Atmos. Chem. Phys.* **2021**, *21* (9), 6721−6734.
(37) Mao, H.; Cheng, I.; Zhang, L. Current understanding of the driving mechanisms for spatiotemporal variations of atmospheric speciated mercury: a review. *Atmos. Chem. Phys.* **2016**, *16* (20), 12897−12924.
(38) Xu, H.; Sonke, J. E.; Guinot, B.; Fu, X.; Sun, R.; Lanzanova, A.; Candaudap, F.; Shen, Z.; Cao, J. Seasonal and Annual Variations in Atmospheric Hg and Pb Isotopes in Xi'an, China. *Environ. Sci. Technol.* **2017**, *51* (7), 3759−3766.
(39) Fu, X.; Zhang, H.; Feng, X.; Tan, Q.; Ming, L.; Liu, C.; Zhang, L. Domestic and Transboundary Sources of Atmospheric Particulate Bound Mercury in Remote Areas of China: Evidence from Mercury Isotopes. *Environ. Sci. Technol.* **2019**, *53* (4), 1947−1957.
(40) Yuan, S.; Chen, J.; Cai, H.; Yuan, W.; Wang, Z.; Huang, Q.; Liu, Y.; Wu, X. Sequential samples reveal significant variation of mercury isotope ratios during single rainfall events. *Sci. Total Environ.* **2018**, *624*, 133−144.
(41) Gratz, L. E.; Keeler, G. J.; Blum, J. D.; Sherman, L. S. Isotopic Composition and Fractionation of Mercury in Great Lakes Precipitation and Ambient Air. *Environ. Sci. Technol.* **2010**, *44* (20), 7764−7770.
(42) Yuan, S.; Zhang, Y.; Chen, J.; Kang, S.; Zhang, J.; Feng, X.; Cai, H.; Wang, Z.; Wang, Z.; Huang, Q. Large Variation of Mercury Isotope Composition During a Single Precipitation Event at Lhasa City, Tibetan Plateau, China. *Procedia Earth Planet. Sci.* **2015**, *13*, 282−286.
(43) Li, X.; Li, Z.; Wu, T.; Chen, J.; Fu, C.; Zhang, L.; Feng, X.; Fu, X.; Tang, L.; Wang, Z.; Wang, Z. Atmospheric mercury emissions from two pre-calciner cement plants in Southwest China. *Atmos. Environ.* **2019**, *199*, 177−188.
(44) Sun, R.; Cao, F.; Dai, S.; Shan, B.; Qi, C.; Xu, Z.; Li, P.; Liu, Y.; Zheng, W.; Chen, J. Atmospheric Mercury Isotope Shifts in Response to Mercury Emissions from Underground Coal Fires. *Environ. Sci. Technol.* **2023**, *57* (23), 8638−8649.
(45) Fu, X.; Yang, X.; Tan, Q.; Ming, L.; Lin, T.; Lin, C.-J.; Li, X.; Feng, X. Isotopic Composition of Gaseous Elemental Mercury in the Marine Boundary Layer of East China Sea. *J. Geophys. Res.* **2018**, *123*, 7656.
(46) Demers, J. D.; Sherman, L. S.; Blum, J. D.; Marsik, F. J.; Dvonch, J. T. Coupling atmospheric mercury isotope ratios and meteorology to identify sources of mercury impacting a coastal urban-industrial region near Pensacola, Florida, USA. *Global Biogeochem. Cycles* **2015**, *29* (10), 1689−1705.
(47) Yuan, W.; Wang, X.; Lin, C. J.; Sommar, J. O.; Wang, B.; Lu, Z.; Feng, X. Quantification of Atmospheric Mercury Deposition to and Legacy Re-emission from a Subtropical Forest Floor by Mercury Isotopes. *Environ. Sci. Technol.* **2021**, *55* (18), 12352−12361.
(48) Zhang, L.; Wang, S. X.; Wang, L.; Hao, J. M. Atmospheric mercury concentration and chemical speciation at a rural site in Beijing, China: implications of mercury emission sources. *Atmos. Chem. Phys.* **2013**, *13* (20), 10505−10516.
(49) Gao, W.; Jiang, W.; Zhou, M. The spatial and temporal characteristics of mercury emission from coal combustion in China during the year 2015. *Atmos. Pollut. Res.* **2019**, *10* (3), 776−783.
(50) Cui, Z.; Li, Z.; Zhang, Y.; Wang, X.; Li, Q.; Zhang, L.; Feng, X.; Li, X.; Shang, L.; Yao, Z. Atmospheric Mercury Emissions from Residential Coal Combustion in Guizhou Province, Southwest China. *Energy Fuels* **2019**, *33* (3), 1937−1943.
(51) Kurz, A. Y.; Blum, J. D.; Johnson, M. W.; Nadelhoffer, K.; Zak, D. R. Isotopic composition of mercury deposited via snow into mid-latitude ecosystems. *Sci. Total Environ.* **2021**, *784*, 147252.
(52) Chen, J. Atmospheric Mercury Emissions and Isotopic Characteristics of NSP Cement Plants, Master Thesis; Guizhou Normal University, 2017.
(53) Sun, R.; Sonke, J. E.; Heimburger, L. E.; Belkin, H. E.; Liu, G.; Shome, D.; Cukrowska, E.; Liousse, C.; Pokrovsky, O. S.; Streets, D. G. Mercury stable isotope signatures of world coal deposits and historical coal combustion emissions. *Environ. Sci. Technol.* **2014**, *48* (13), 7660−7668.
(54) Yin, R.; Feng, X.; Chen, J. Mercury stable isotopic compositions in coals from major coal producing fields in China and their geochemical and environmental implications. *Environ. Sci. Technol.* **2014**, *48* (10), 5565−5574.
(55) Sun, G.; Sommar, J.; Feng, X.; Lin, C. J.; Ge, M.; Wang, W.; Yin, R.; Fu, X.; Shang, L. Mass-Dependent and -Independent Fractionation of Mercury Isotope during Gas-Phase Oxidation of Elemental Mercury Vapor by Atomic Cl and Br. *Environ. Sci. Technol.* **2016**, *50* (17), 9232−9241.
(56) Sun, R. Mercury Stable Isotope Fractionation During Coal Combustion in Coal-Fired Boilers: Reconciling Atmospheric Hg Isotope Observations with Hg Isotope Fractionation Theory. *Bull. Environ. Contam. Toxicol.* **2019**, *102* (5), 657−664.

https://doi.org/10.1021/acs.est.4c07649
Environ. Sci. Technol. 2024, 58, 16855−16866

(57) Sun, R.; Heimbürger, L.-E.; Sonke, J. E.; Liu, G.; Amouroux, D.; Berail, S. Mercury stable isotope fractionation in six utility boilers of two large coal-fired power plants. *Chem. Geol.* **2013**, *336*, 103−111.
(58) Ouyang, D.; Wu, Q.; Li, G.; Han, D.; Wang, S. Impacts of Material Input and Production Process on the Isotopic Fingerprint of Atmospheric Mercury Emissions from Cement Clinker Production. *Environ. Sci. Technol. Lett.* **2022**, *9* (11), 900−905.
(59) Lohman, K.; Seigneur, C.; Edgerton, E.; Jansen, J. Modeling mercury in power plant plumes. *Environ. Sci. Technol.* **2006**, *40* (12), 3848−3854.
(60) Edgerton, E. S.; Hartsell, B. E.; Jansen, J. J. Mercury speciation in coal-fired power plant plumes observed at three surface sites in the southeastern US. *Environ. Sci. Technol.* **2006**, *40* (15), 4563−4570.
(61) Deeds, D. A.; Banic, C. M.; Lu, J.; Daggupaty, S. Mercury speciation in a coal-fired power plant plume: An aircraft-based study of emissions from the 3640 MW Nanticoke Generating Station, Ontario, Canada. *J. Geophys. Res.* **2013**, *118* (10), 4919−4935.
(62) Weigelt, A.; Slemr, F.; Ebinghaus, R.; Pirrone, N.; Bieser, J.; Bödewadt, J.; Esposito, G.; van Velthoven, P. F. J. Mercury emissions of a coal-fired power plant in Germany. *Atmos. Chem. Phys.* **2016**, *16* (21), 13653−13668.
(63) Zhang, Y.; Jacob, D. J.; Horowitz, H. M.; Chen, L.; Amos, H. M.; Krabbenhoft, D. P.; Slemr, F.; St Louis, V. L.; Sunderland, E. M. Observed decrease in atmospheric mercury explained by global decline in anthropogenic emissions. *Proc. Natl. Acad. Sci. U.S.A.* **2016**, *113* (3), 526−531.
(64) Horowitz, H. M.; Jacob, D. J.; Zhang, Y.; Dibble, T. S.; Slemr, F.; Amos, H. M.; Schmidt, J. A.; Corbitt, E. S.; Marais, E. A.; Sunderland, E. M. A new mechanism for atmospheric mercury redox chemistry: implications for the global mercury budget. *Atmos. Chem. Phys.* **2017**, *17* (10), 6353−6371.
(65) Zhu, W.; Fu, X.; Zhang, H.; Liu, C.; Skyllberg, U.; Sommar, J.; Yu, B.; Feng, X. Mercury Isotope Fractionation during the Exchange of Hg(0) between the Atmosphere and Land Surfaces: Implications for Hg(0) Exchange Processes and Controls. *Environ. Sci. Technol.* **2022**, *56* (2), 1445−1457.
(66) Shah, V.; Jacob, D. J.; Thackray, C. P.; Wang, X.; Sunderland, E. M.; Dibble, T. S.; Saiz-Lopez, A.; Černušák, I.; Kellö, V.; Castro, P. J.; Wu, R.; Wang, C. Improved Mechanistic Model of the Atmospheric Redox Chemistry of Mercury. *Environ. Sci. Technol.* **2021**, *55* (21), 14445−14456.
(67) Nguyen, L. S. P.; Sheu, G.-R.; Fu, X.; Feng, X.; Lin, N.-H. Isotopic composition of total gaseous mercury at a high-altitude tropical forest site influenced by air masses from the East Asia continent and the Pacific Ocean. *Atmos. Environ.* **2021**, *246*, 118110.
(68) Sun, G.; Feng, X.; Yin, R.; Wang, F.; Lin, C. J.; Li, K.; Sommar, J. O. Dissociation of Mercuric Oxides Drives Anomalous Isotope Fractionation during Net Photo-oxidation of Mercury Vapor in Air. *Environ. Sci. Technol.* **2022**, *56* (18), 13428−13438.
(69) Qin, X.; Guo, Q.; Martens, P.; Krafft, T. Mercury stable isotopes revealing the atmospheric mercury circulation: A review of particulate bound mercury in China. *Earth-Sci. Rev.* **2024**, *250*, 104681.
(70) Cai, X.; Cai, B.; Zhang, H.; Chen, L.; Zheng, C.; Tong, P.; Lin, H.; Zhang, Q.; Liu, M.; Tong, Y.; Wang, X. Establishment of High-Resolution Atmospheric Mercury Emission Inventories for Chinese Cement Plants Based on the Mass Balance Method. *Environ. Sci. Technol.* **2020**, *54* (21), 13399−13408.

https://doi.org/10.1021/acs.est.4c07649
Environ. Sci. Technol. 2024, 58, 16855−16866